

# SCIENTIFIC REPORTS



OPEN

## LOXL2 drives epithelial-mesenchymal transition via activation of IRE1-XBP1 signalling pathway

Received: 05 September 2016

Accepted: 17 February 2017

Published: 23 March 2017

Eva P. Cuevas<sup>1</sup>, Pilar Eraso<sup>1</sup>, María J. Mazón<sup>1</sup>, Vanesa Santos<sup>1</sup>, Gema Moreno-Bueno<sup>1,2</sup>, Amparo Cano<sup>1</sup> & Francisco Portillo<sup>1</sup>

Epithelial-to-Mesenchymal Transition (EMT) is a key process contributing to the aggressiveness of cancer cells. EMT is triggered by activation of different transcription factors collectively known as EMT-TFs. Different cellular cues and cell signalling networks activate EMT at transcriptional and posttranscriptional level in different biological and pathological situations. Among them, overexpression of LOXL2 (lysyl oxidase-like 2) induces EMT independent of its catalytic activity. Remarkably, perinuclear/cytoplasmic accumulation of LOXL2 is a poor prognosis marker of squamous cell carcinomas and is associated to basal breast cancer metastasis by mechanisms no yet fully understood. Here, we report that overexpression of LOXL2 promotes its accumulation in the Endoplasmic Reticulum where it interacts with HSPA5 leading to activation of the IRE1-XBP1 signalling pathway of the ER-stress response. LOXL2-dependent IRE1-XBP1 activation induces the expression of several EMT-TFs: *SNAI1*, *SNAI2*, *ZEB2* and *TCF3* that are direct transcriptional targets of XBP1. Remarkably, inhibition of IRE1 blocks LOXL2-dependent upregulation of EMT-TFs thus hindering EMT induction.

Epithelial-to-Mesenchymal Transition (EMT) is an essential program designed to promote migration of specific cells at different development stages such as during mesoderm formation and migration of neural crest cells<sup>1</sup>. Unfortunately, during the progression of solid human tumours, EMT is abnormally activated providing cancer cells with the ability to invade adjacent tissues and form distant metastasis. Hallmarks of EMT are the loss of E-cadherin and other epithelial markers, loss of cell-cell junctions and apico-basal cell polarity concomitant to the acquisition of migration and stem cell properties<sup>2-7</sup>. Studies from different groups have led to the identification of several E-cadherin transcriptional repressors and EMT-inducers (collectively known as EMT-TFs), such as the zinc finger factors *SNAIL1* and *SNAIL2*, the two-handed zinc finger proteins *ZEB1* and *ZEB2* and the bHLH factors *E12/E47* (*TCF3*), *E2-2* (*TCF4*) and *TWIST1*<sup>1,8,9</sup> that are regulated at transcriptional, posttranscriptional and posttranslational levels<sup>2,7,9,10</sup>. Recent studies in breast and pancreatic cancer models suggest that EMT contributes to tumour malignancy by increasing their chemo-resistance instead of contributing to metastasis<sup>11,12</sup> thus adding more complexity to the understanding of tumour progression.

We previously described that intracellular lysyl oxidase-like 2 (LOXL2) is able to induce EMT<sup>13</sup> independently of its catalytic activity<sup>14</sup> and identified intracellular LOXL2 as a poor prognosis marker of laryngeal squamous cell carcinomas<sup>15</sup> and basal-like breast carcinomas<sup>16</sup>. Moreover, different carcinoma cell lines exhibit high levels of LOXL2 and its silencing attenuates their invasive cell phenotype<sup>17,18</sup>.

LOXL2 is a member of the lysyl oxidase (LOX) family that belongs to the lysine-tyrosylquinone (LTQ)-dependent copper amine oxidases. The LOX protein family consists of five members including LOX, and four LOX-like paralogs LOXL1, LOXL2, LOXL3 and LOXL4<sup>19-21</sup>. All the members of the family share a highly conserved C-terminal catalytic domain responsible for the oxidative deamination of peptidyl-lysine residues required for covalent inter and intramolecular crosslinking of substrates, as extracellular matrix (ECM)

<sup>1</sup>Departamento de Bioquímica, Universidad Autónoma de Madrid (UAM), Instituto de Investigaciones Biomédicas "Alberto Sols" (CSIC-UAM), IdiPAZ, CIBERONC, Madrid, Spain. <sup>2</sup>Fundación MD Anderson International, Madrid, Spain. Correspondence and requests for materials should be addressed to F.P. (email: fportillo@iib.uam.es) or A.C. (email: acano@iib.uam.es)

components<sup>19,22</sup>. The N-terminus is more divergent among the LOXL family members and includes, in the case of LOXL2, LOXL3 and LOXL4, four Scavenger Receptor Cysteine-Rich (SRCR) domains<sup>23</sup> characterized by the presence of three disulphide bonds<sup>24</sup>. One structural feature of LOXL2 is the presence of three N-linked glycans required for proper folding of the protein<sup>25</sup>. Although LOXL2 was initially described as a secreted protein involved in the ECM maturation<sup>26–30</sup>, novel LOXL2 functions associated to a perinuclear and nuclear localization have also been described<sup>13,31,32</sup> and involved in different pathological processes as in cancer<sup>15,16,17,33–38</sup>.

Secretory proteins, like LOXL2, are co-translationally translocated into the Endoplasmic Reticulum (ER) where they undergo different maturation processes before ER export<sup>39,40</sup>. Disruption of protein maturation in the ER causes ER stress and activates an adaptive mechanism termed Unfolded Protein Response (UPR) aimed to restore ER homeostasis<sup>41</sup>. Activation of the UPR has been observed in different metabolic diseases and in cancer<sup>42–44</sup>. In mammals, UPR is mediated by three independent stress sensors localized at the ER membrane. Each sensor distinguishes a different branch of the UPR: PERK-eIF2 $\alpha$ , IRE1-XBP1 and ATF6. The activity of the three stress sensors is controlled by the ER-resident chaperone HSPA5 (also known as GRP78 and BIP) that binds to IRE1, PERK and ATF6 and negatively regulates their activity<sup>41,45,46</sup>. Upon ER stress, accumulated unfolded proteins force HSPA5 dissociation and the consequent IRE1, PERK and ATF6 activation. Each activated sensor triggers an independent UPR signalling branch<sup>47</sup>. Thus, activated IRE1 induces specific splicing of a 26 base pair intron of *XBP1* mRNA, causing active XBP1 transcription factor that upregulates target genes, such as *EDEM1* and *DNAJB9*<sup>48</sup>. In turn, activated PERK phosphorylates eIF2 $\alpha$ , turning off protein synthesis but selectively increasing the translation of ATF4 transcription factor<sup>49</sup>. Finally, activated ATF6 translocates to the Golgi where it is sequentially cleaved by the site-1 and site-2 proteases, releasing an N-terminal fragment that acts as an active transcription factor<sup>50,51</sup>.

LOXL2 is posttranslationally modified in the ER in several ways i.e.: disulphide bond formation (at least twelve, three for each SRCR domain and most likely additional five for the catalytic domain), three N-glycans addition, Cu<sup>2+</sup> coordination and LTQ autocatalytic formation, all of them being expected to be essential for the maturation of the enzyme and thus for its ER exit<sup>19,24,25</sup>. Based on the posttranslational features of LOXL2 we hypothesized that the perinuclear localization of the protein in human tumours could reflect LOXL2 accumulation in the ER because under overexpression conditions the posttranslational processing turns out to be a limiting step. We therefore asked whether such LOXL2 ER overload could cause ER stress and also inquired about its contribution to LOXL2-dependent EMT induction.

Here, we report that overexpression of LOXL2 causes ER overload that activates the IRE1-XBP1 and PERK branches of the UPR and drives EMT via XBP1-mediated upregulation of *SNAI1*, *SNAI2*, *ZEB2* and *TCF3*. Importantly, inhibition of IRE1 blocks the capacity of LOXL2 to induce EMT-TFs upregulation and, thus, to trigger EMT.

## Results

**ER overload upon LOXL2 overexpression.** To assess the consequences of increased LOXL2 expression on its cellular localization two complementary approaches were undertaken. In the first one, the localization of endogenous LOXL2 in MDA-MB-231 and Hs578T basal-like carcinoma cell lines expressing high levels of LOXL2<sup>16</sup> was analysed by Optiprep gradient centrifugation and confocal immunofluorescence. In both cases, Calnexin and GM130 were used as ER and cis-Golgi markers, respectively. LOXL2 co-fractionated mainly with Calnexin in the lineal Optiprep gradients (Fig. 1a,b) and immunofluorescence analysis confirmed LOXL2 co-localization with Calnexin-positive ER structures in both cell lines (Fig. 1c,d). As a second approach we investigated the localization of LOXL2 in MDCK-II cells stably expressing wild-type LOXL2 or one catalytic inactive mutant ( $\Delta$ LOXL2)<sup>14</sup>. Both wild-type LOXL2 and mutant  $\Delta$ LOXL2 co-fractionated and co-localized mostly with ER markers under overexpression conditions (Supplementary Fig. 1). In both approaches a minor fraction of LOXL2 co-localized with the Golgi marker likely corresponding to LOXL2 leaving the ER.

**LOXL2 interacts with HSPA5 and activates the IRE1-XBP1 signalling pathway.** To get insights into the mechanisms of LOXL2 retention in ER, we next investigated the interactome of LOXL2. To this end, whole cell extracts from HEK293T cells overexpressing a Flag-tagged version of LOXL2 were immunoprecipitated with anti-Flag M2 affinity gel and proteins were identified by mass spectrometry. Among the proteins immunoprecipitated with LOXL2 showing a high score, HSPA5 draw our attention because of its role in the folding and assembly of proteins in the ER and as a regulator of the UPR<sup>41,46</sup> (Supplementary Fig. 2a). We, next, confirmed the LOXL2/HSPA5 interaction by co-immunoprecipitation in HEK293T cells ectopically expressing LOXL2 (Supplementary Fig. 2b) as well as in Hs578T cells endogenously expressing LOXL2 (Supplementary Fig. 2c).

Given the key role of HSPA5 in the control of UPR<sup>41,46</sup> we hypothesized that the interaction between LOXL2 and HSPA5 may activate the UPR by sequestering HSPA5 from the stress sensors. To investigate this aspect, we analysed the expression of two well characterized reporter systems in which the luciferase gene is under the control of three copies of the cis-regulatory elements *UPRE* (Unfolded Protein Response Element, and preferential binding site of activated/spliced XBP1) or *ERSE* (ER-Stress Response Element, binding site for of XBP1 and ATF6)<sup>52</sup>. Upon LOXL2 and  $\Delta$ LOXL2 overexpression both reporters were transactivated at levels similar to those obtained with tunicamycin, a classical ER stressor<sup>53</sup> (Fig. 2a). As a control, the overexpression of the extracellular protein ANXA2, which exhibited the same co-localization pattern than LOXL2 (Supplementary Fig. 3), did not transactivate the reporters (Fig. 2a). We then assessed the potential regulatory effect of LOXL2 on the UPR response by analysing the transcriptome of MDCK-II cells stably expressing LOXL2 or  $\Delta$ LOXL2 compared to control cells transfected with the empty plasmid. We found 337 genes that displayed a > 2.0 fold change in expression with respect to the control cells, the majority of them (330) common to LOXL2 or  $\Delta$ LOXL2 overexpressing cells (Supplementary Dataset). As expected E-cadherin (*CDH1*) was downregulated in both cell lines (Supplementary Dataset). Analysis of the expression pattern in independent gene expression data sets (Gene

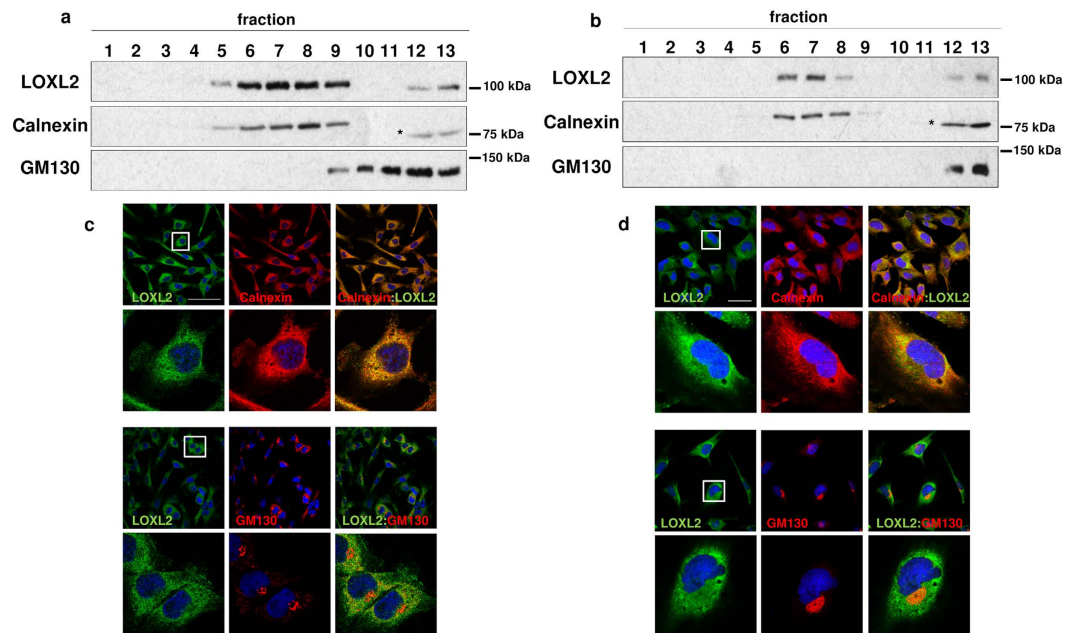


**Figure 1. Accumulation of LOXL2 in the ER.** (a,b) Total membrane fractions from MDA-MB-231 (a) and Hs578T (b) cells were fractionated on linear Optiprep gradients and fractions were analysed by immunoblotting using anti-LOXL2 (Origene), and anti-Calnexin and anti-GM130 as ER and cis-Golgi markers, respectively. (\*) Unrelated protein. (c,d) Immunofluorescence staining of LOXL2 (green), Calnexin and GM130 (red) in MDA-MB-231 (c) and Hs578T (d) cells; merge images are shown on the right panels. Nuclei were counterstained with DAPI (blue); scale bars, 50  $\mu$ m. Insets in c and d, indicate amplified areas shown in the bottom panels.

Expression Atlas; <http://www.ebi.ac.uk/gxa/home>) revealed that 36% (120 out of 330; underlined) and 30% (99 out of 330; bold) of the genes were also commonly regulated in cells treated with tunicamycin or thapsigargin, respectively (Supplementary Dataset), two classic UPR activators<sup>53</sup>.

We next interrogated whether overexpression of LOXL2/ $\Delta$ LOXL2 in HEK293T cells is able to activate the UPR canonical branches (Fig. 2b). We first examined the activation status of IRE1, PERK and ATF6 in HEK293T-LOXL2/ $\Delta$ LOXL2 cells compared to controls. IRE1 activation was probed by analysing *XBP1* splicing; PERK activation by evaluating EIF2 $\alpha$  phosphorylation level and ATF6 activation by measuring the amount of processed ATF6. LOXL2 and  $\Delta$ LOXL2 overexpression clearly promoted *XBP1* splicing (Fig. 2c) and increased EIF2 $\alpha$  phosphorylation level, but had not significant effect on the amount of processed ATF6 (detected as a protein of about 50 kDa) (Fig. 2d). These results suggest that overexpression of LOXL2 is activating the IRE1 and PERK branches of the UPR. We next analysed by qPCR the expression of the *XBP1* target genes, *EDEM1* and *DNAJB9*<sup>54</sup>. The level of ATF4, a preferential translational target of phosphorylated EIF2 $\alpha$ , was evaluated indirectly by analysing the expression levels of the ATF4 target gene *DDIT3*<sup>55,56</sup>. Additionally, we analysed the expression of the ATF6 target gene *SEL1L*<sup>57</sup>. LOXL2 and  $\Delta$ LOXL2 overexpression significantly increased the expression of *EDEM1*, *DNAJB9* and *DDIT3* and had not significant effect on the expression of *SEL1L* (Fig. 2e).

Together, the above data suggest that LOXL2 and  $\Delta$ LOXL2 are able to activate the IRE1 and PERK branches of UPR. Next, we evaluated the consequences of IRE1 inhibition on the observed LOXL2-dependent upregulation of *XBP1* splicing and upregulation of *XBP1* target genes. To this end, HEK293T cells overexpressing LOXL2 were treated with the specific IRE1 inhibitor 4 $\mu$ 8 C<sup>58</sup> and the degree of *XBP1* splicing and *EDEM1* and *DNAJB9* mRNA levels analysed; as positive controls HEK293T cells transfected with empty vector were treated with tunicamycin and/or 4 $\mu$ 8 C. Inhibition of IRE1 fully blocked the LOXL2 mediated upregulation of *XBP1* splicing and, concomitantly, hampered LOXL2 upregulation of *EDEM1* and *DNAJB9* expression, similar to the inhibition of those parameters induced by tunicamycin (Fig. 2f and Supplementary Fig. 4). A similar result was obtained with  $\Delta$ LOXL2 (see next Results subsection).

To provide additional evidence of the functional link of LOXL2 to IRE1-*XBP1* activation, we tested the effect of LOXL2 knockdown on *XBP1* splicing and *UPRE* and *ERSE* reporters activation. When LOXL2 was knocked down in two independent breast cancer cell lines, Eo771 and MDA-MB-231 expressing high endogenous LOXL2 levels<sup>16,59</sup>, *XBP1* splicing and transactivation of the *UPRE* and *ERSE* gene reporters were abrogated or strongly decreased in both cell lines (Fig. 3a,b).

**IRE1-*XBP1* activation induces EMT through upregulation of EMT-TFs.** Based on the fact that MDCK-II cells overexpressing LOXL2 have undergone an EMT process, upregulate the IRE1-*XBP1* pathway and exhibit increased *TWIST1* and *ZEB1* expression (Supplementary Dataset), we speculated that IRE1-*XBP1* activation could upregulate the expression of some of the EMT-TFs to trigger EMT. To assess this, we investigated

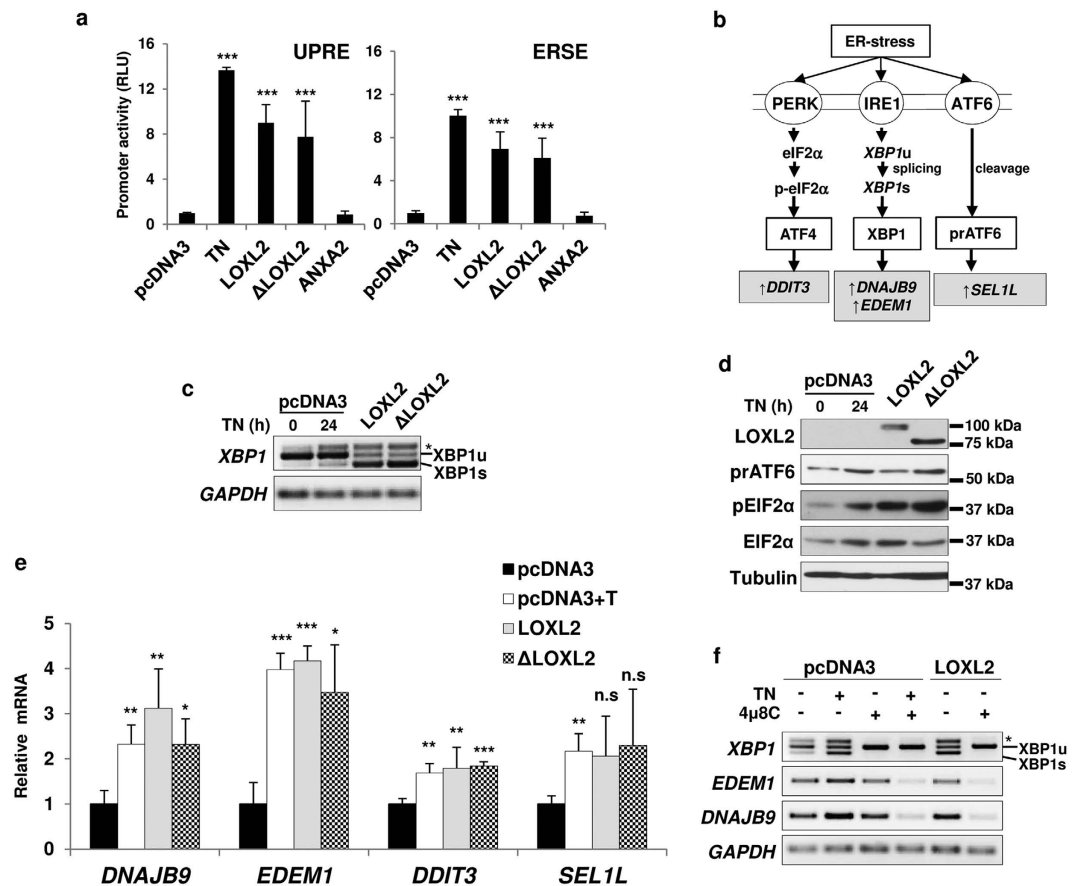


**Figure 2. LOXL2 regulates IRE1-XBP1 branch of the UPR.** (a) LOXL2 and  $\Delta$ LOXL2 but not ANXA2 enhance p5xUPRE-GL3 (UPRE) (left) and pGL3-GRP78P(-132)-luc (ERSE) (right) reporters activity. Promoter activities were analysed by luciferase reporter assays in HEK293T cells. As control, luciferase activities were analysed in cells co-transfected with the empty plasmid (pcDNA3) and treated with tunicamycin (TN). Error bars represent s.e.m. (n = 6) (\*\*p < 0.01, \*\*\*p < 0.001). (b) Schematic diagram illustrating the UPR branches. Circles, ER-stress sensors; white squares, ER-stress activated transcription factors; grey squares, target genes. (c) XBP1 splicing is induced by LOXL2 and  $\Delta$ LOXL2. RT-PCR analysis of XBP1 splicing in HEK293T cells transiently transfected with pcDNA3-LOXL2 and - $\Delta$ LOXL2. As control, XBP1 splicing was analysed in cells transfected with empty plasmid (pcDNA3) and treated with tunicamycin (TN) for 24 h. GAPDH levels serve as loading control. Unspliced (XBP1u) and spliced (XBP1s) forms of XBP1 are indicated. (\*) XBP1 hybrid band<sup>70</sup>. One representative RT-PCR analysis of fourth independent experiments is shown. (d) PERK- but not ATF6-branch is activated by LOXL2 and  $\Delta$ LOXL2. Cells used in (c) were processed for WB using antibodies against LOXL2 (K. Csiszar), processed ATF6 (prATF6), phosphoEIF2 $\alpha$  (pEIF2 $\alpha$ ) and total EIF2 $\alpha$  (EIF2 $\alpha$ ).  $\alpha$ -tubulin was used as loading control. One representative blot of two independent experiments is shown. (e) LOXL2 and  $\Delta$ LOXL2 mostly upregulate XBP1 target genes expression. Cells used in (c) were processed for qPCR analysis of the indicated genes. GAPDH levels serve as internal control. Results show s.e.m. of four independent experiments performed on triplicate samples; (\*p < 0.05, \*\*p < 0.01, \*\*\*p < 0.001, n.s. not significant). (f) LOXL2-dependent XBP1 activation is mediated by IRE1. RT-PCR analysis of XBP1 splicing and XBP1 target genes expression was performed in HEK293T cells transiently transfected with pcDNA3-LOXL2 and treated with the IRE1 inhibitor 4 $\mu$ 8 C. As control, cells transfected with the empty plasmid (pcDNA3) and treated with tunicamycin (TN) and/or 4 $\mu$ 8 C were used. GAPDH levels serve as internal control. One representative RT-PCR analysis of two independent experiments is shown.

whether the expression levels of the classical EMT-TFs *SNAI1*, *SNAI2*, *ZEB1*, *ZEB2*, *TCF3* and *TWIST1*<sup>17</sup> are influenced by the activation status of IRE1-XBP1. To this end, we examined the expression levels of the above-mentioned EMT-TFs in HEK293T cells transiently expressing LOXL2 or  $\Delta$ LOXL2 and treated or not with 4 $\mu$ 8 C. In parallel, we analysed the EMT-TFs expression levels in cells transfected with empty plasmid (pcDNA3) and treated with tunicamycin  $\pm$  4 $\mu$ 8 C. As control of IRE1-XBP1 activation we evaluated the degree of XBP1 splicing and the *EDEM1* and *DNAJB9* expression levels. Consistent with IRE1-XBP1 activation, the upregulation of XBP1 splicing and increased *EDEM1* and *DNAJB9* expression levels caused by tunicamycin or LOXL2 variants was abrogated by 4 $\mu$ 8 C treatment (Fig. 4a). Remarkably, strong upregulation of all analysed EMT-TFs was observed in cells overexpressing LOXL2 or  $\Delta$ LOXL2, even at higher levels than those induced by tunicamycin, and fully counteracted by 4 $\mu$ 8 C treatment (Fig. 4a). It is worth mentioning that despite the low  $\Delta$ LOXL2

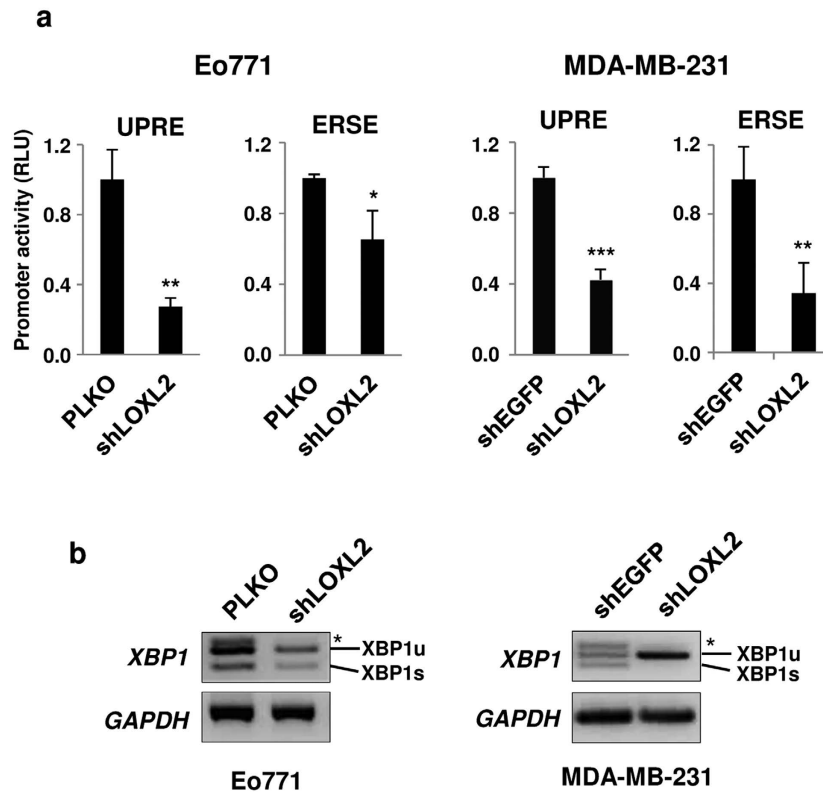


**Figure 3. LOXL2 depletion diminishes UPR and ERSE promoter activities in breast carcinoma cells.** (a) Promoter assays were performed in control mouse Eo771 (pLKO) (left) and in cells silenced for LOXL2 (shLOXL2) (right) and in cells silenced for LOXL2 (shLOXL2). Error bars represent the s.e.m. (n = 3) (\*p < 0.05, \*\*p < 0.01, \*\*\*p < 0.001). (b) LOXL2 knockdown in Eo771 and MDA-MB-231 cells abrogates *XBP1* splicing. Cells used in (a) were processed for RT-PCR analysis of spliced *XBP1*. *GAPDH* levels serve as loading control. Unspliced (*XBP1u*) and spliced (*XBP1s*) forms of *XBP1* are indicated. (\*) *XBP1* hybrid band. One representative RT-PCR analysis of three independent experiments is shown.

mRNA levels detected compared to wild-type *LOXL2* mRNA both forms were detected at similar protein levels in whole cell extracts (Supplementary Fig. 5). These data suggest that *LOXL2*-dependent upregulation of EMT-TFs is specific of the IRE1-XBP1 branch. Next, we scanned the promoter regions of the EMT-TFs for XBP1 binding sites using P-Match software (www.gene-regulation.com) and found putative XBP1 binding sites (*UPRE* core motif ACGTG)<sup>54</sup> in *SNAI1* (position -550), *SNAI2* (position -526), *ZEB2* (positions -2269 and -658) and *TCF3* (position -2230) promoters. We then analysed the binding of a Flag-tagged version of the processed XBP1 (*XBP1p*) to the endogenous *SNAI1*, *SNAI2*, *TCF3* and *ZEB2* promoters by chromatin immunoprecipitation (ChIP) assays showing that indeed XBP1 interacts with the four promoters as well as with the *HSPA5* promoter, used as control<sup>54</sup> (Fig. 4b). To probe the functionality of XBP1-EMT-TF promoter interactions, we next performed luciferase reporter assays on the *SNAI2* and *TCF3* promoters. HEK293T cells were then transfected with the processed form of XBP1 (*XBP1p*), *LOXL2* or  $\Delta$ *LOXL2* and either the *SNAI2* (p*SNAI2*) or the *TCF3* (p*TCF3*) promoters fused to luciferase. As can be observed in Fig. 4c and d, *XBP1p*, *LOXL2* and  $\Delta$ *LOXL2* significantly increased *SNAI2* and *TCF3* promoter activities, supporting that those EMT-TFs are direct targets of *XBP1p*. As control, tunicamycin treated cells showed increased activity of *TCF3* promoter but not significant change in *SNAI2* promoter (Fig. 4c), in agreement with the mRNA levels of both EMT-TFs observed in tunicamycin treated cells (Fig. 4a).

Taken together, these results strongly suggest that wild-type *LOXL2* or  $\Delta$ *LOXL2* overexpression activates the IRE1-XBP1 branch of the UPR that in turn upregulates the expression of EMT-TFs leading to EMT induction.

**Inhibition of IRE1 blocks the EMT induced by LOXL2.** We finally interrogated whether inhibition of the IRE1-XBP1 branch could prevent the *LOXL2*-dependent induction of EMT. To this end, MDCK-II cells expressing the tetracycline- transactivator tTA were stably transfected with a plasmid carrying *LOXL2* under the control of a TET-regulatable promoter. After *LOXL2* induction we analysed the impact of the IRE1 inhibitor 4 $\mu$  8 C on the dynamics of the EMT fostered by *LOXL2* in two independent clones (Fig. 5 and Supplementary Fig. 6). In the absence of inhibitor a marked decrease in E-cadherin levels and expression of the mesenchymal markers N-cadherin, fibronectin and vimentin was detected after 1 week of *LOXL2* induction and was maintained up to 3 weeks (Fig. 5). Noticeably, the changes in EMT marker expression were blocked or substantially reduced in the presence of 4 $\mu$  8 C (Fig. 5a). In agreement with those observations, the IRE1 inhibitor hampered the acquisition of the spindle phenotype characteristic of cells suffering an EMT, as observed in control *LOXL2*-induced cells

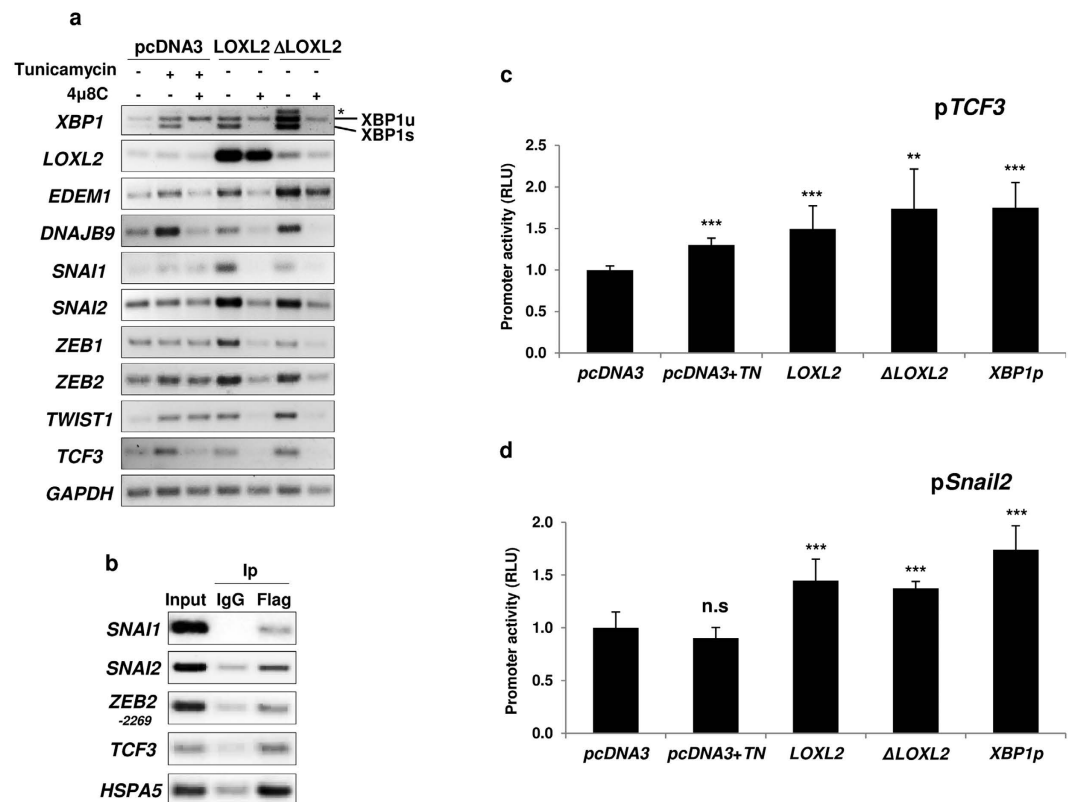


**Figure 4. Activation of the IRE1-XBP1 branch by LOXL2 upregulates the expression of EMT-TFs.** (a) IRE1 activation increases the expression of EMT-TFs. RT-PCR analysis of the expression level of EMT-TFs (*SNAI1*, *SNAI2*, *ZEB1*, *ZEB2*, *TWIST1* and *TCF3*) in HEK293T cells transiently transfected with pcDNA3-*LOXL2* and - $\Delta$ *LOXL2* and treated or not with 4  $\mu$ 8C. As control, RT-PCR analysis was also performed in cells transfected with empty plasmid (pcDNA3) and treated with tunicamycin and/or 4  $\mu$ 8C. RT-PCR analysis of *XBP1* splicing and expression of *DNAJB9* and *EDEM1* was included as internal control of the activation and inhibition of IRE1. One representative RT-PCR analysis of three independent experiments is shown. (b) XBP1 binds to endogenous *SNAI1*, *SNAI2*, *ZEB2* and *TCF3* gene promoters. Chromatin immunoprecipitation assays were performed in HEK293T cells transiently transfected with a Flag-tagged version of the processed *XBP1* (*XBP1p*) for the indicated EMT-TFs upstream regions. Binding of XBP1p to the *HSPA5* promoter was used as control. One representative PCR analysis of three independent experiments is shown. (c) and (d) XBP1, LOXL2 and  $\Delta$ LOXL2 enhance the activity of the *TCF3* (c) and *SNAI2* (d) gene promoters. *SNAI2* and *TCF3* promoter activities were analysed by luciferase reporter assay in HEK293T cells co-transfected with each reporter plasmid and plasmids expressing processed *XBP1* (*XBP1p*), *LOXL2* or  $\Delta$ *LOXL2*. Promoter activities were normalized to the promoter activity detected in cells transfected with pcDNA3 empty vector. Error bars represent the s.e.m. (n = 4). As control, promoter assays were also performed in cells transfected with empty plasmid (pcDNA3) and treated with tunicamycin. (n = 4) (\*\*p < 0.01, \*\*\*p < 0.001, n.s. not significant).

(Fig. 5b). The blocking of mesenchymal features by inhibition of IRE1 was confirmed by immunofluorescence analysis showing that after 4 weeks of treatment with 4  $\mu$ 8C the epithelial markers E-cadherin and ZO-1 were detected at cell-cell junctions and F-actin acquired a cortical organization typical of epithelial cells, while vimentin levels steadily decrease from 2 to 4 weeks of treatment (Fig. 5c). As expected, in untreated LOXL2-induced cells both epithelial markers were barely detected, vimentin levels remained constant and the F-actin cytoskeleton displayed the stress fibers pattern typical of mesenchymal cells (Fig. 5c). Additionally, we also observed in three independent clones that inhibition of IRE1 blocks the LOXL2-mediated induction of EMT when MDCK-II cells were transfected with LOXL2 and maintained in the presence of the IRE1 inhibitor 4  $\mu$ 8C during four weeks (Supplementary Fig. 7). These results support that inhibition of IRE1 impedes the LOXL2 mediated induction of EMT.

## Discussion

Overexpression of LOXL2 impinges negatively on clinicopathological features of different tumour types<sup>17,18</sup> and is able to induce EMT<sup>13</sup>. Remarkably, we have shown that in human tumour samples LOXL2 is accumulated at discrete areas of the cytoplasm and at the perinuclear region, a cell localization pattern that correlates with poor prognosis of squamous cell carcinomas and distant metastasis of basal breast carcinomas<sup>15,16</sup>. The cell organelles where LOXL2 intracellular accumulation occurs and the physiological/pathological consequences are currently unknown. In this report we show that endogenous or ectopically expressed LOXL2 is mainly localized in the ER.

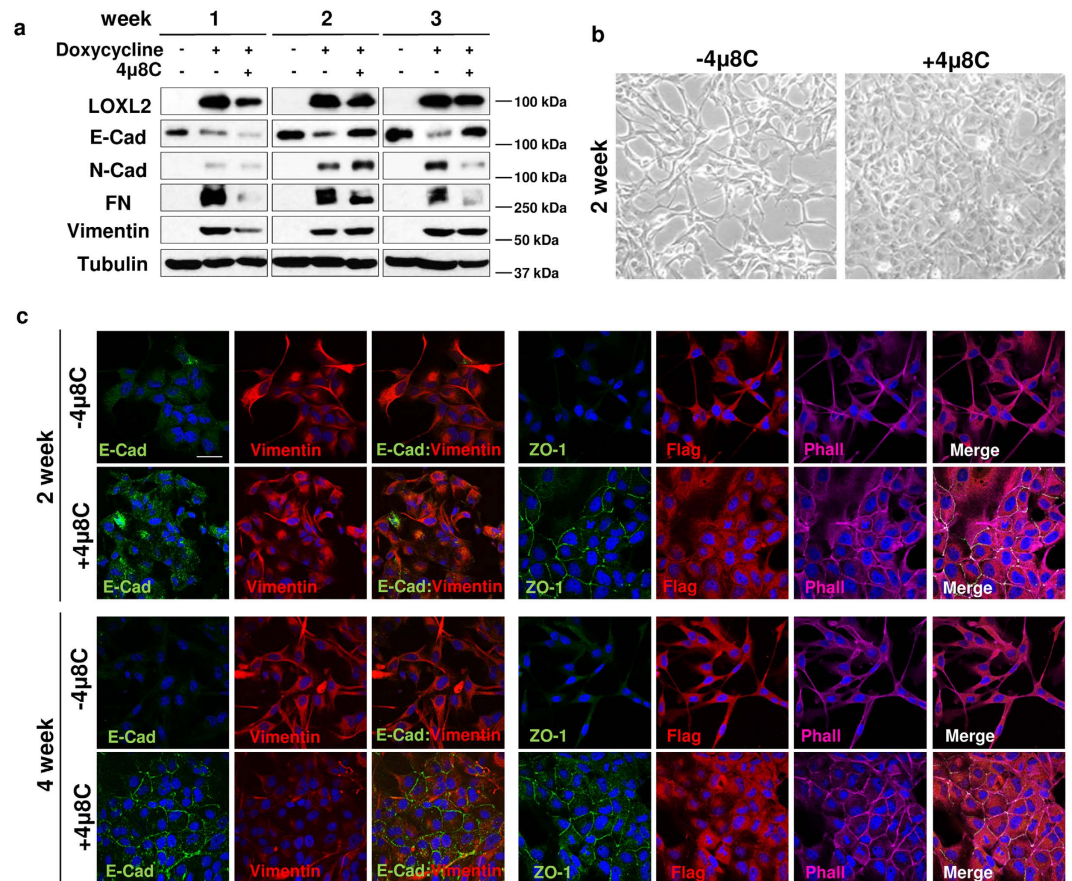


**Figure 5. The IRE1-XBP1 branch of UPR mediates the ability of LOXL2 to induce EMT.** MDCK-II cells with inducible expression of LOXL2-Flag were treated with doxycycline and after that with the IRE1 inhibitor 4μ8C for the indicated time periods. Cells were processed for: (a) WB using antibodies against LOXL2 (anti-Flag), E-cadherin (E-Cad), N-cadherin (N-cad), Fibronectin (FN) and Vimentin.  $\alpha$ -tubulin was used as loading control. One representative blot of two independent experiments is shown. (b) Phase contrast image of the cells after 2 weeks of inhibitor treatment (right) compared to control untreated cells (left). (c) Representative images of confocal immunofluorescence analyses of control and 4μ8C treated cells for the indicated time periods with antibodies against LOXL2 (anti-Flag), E-cadherin (E-cad), ZO-1 and vimentin. F-actin was detected with phalloidin stain. Merge images are shown on the right panels. Scale bars 50 μm.

LOXL2 is posttranslationally modified in the ER in several ways i.e.: disulphide bond formation, N-glycosylation,  $\text{Cu}^{2+}$  coordination and LTQ autocatalytic formation, all of them being essential for the maturation of the enzyme<sup>19,24–25</sup>. We hypothesized that under overexpression conditions, maturation of LOXL2 within the ER could be a bottleneck for its export and, therefore, ER localization of the enzyme could indicate the presence of accumulated precursor forms of LOXL2 waiting for departure from the ER. At present we cannot discriminate the structure of LOXL2 retained in the ER vs the secreted form, with apparent similar molecular mass in denaturing gels. In human tumours with overexpression of LOXL2, the observed regions with intracellular accumulation of LOXL2 could reflect this situation. In neoplastic processes, tumour cells experience different environmental aggressions such as hypoxia, nutrient deprivation, oxidative stress and acidosis that contribute to tumour progression<sup>60</sup>. Although the specific signals/pathways leading to LOXL2 overexpression in tumours are not yet fully characterized, one of the stressful conditions that can trigger LOXL2 overexpression is hypoxia, a very common stress factor in cancer, and in fact LOXL2 gene expression is upregulated by hypoxia and it is a direct target of HIF-1<sup>61</sup>.

In the ER, upon LOXL2 interaction with HSPA5 the IRE1-XBP1 and PERK branches of the UPR are activated. On the other hand, the ATF6 sensor was not activated by LOXL2. This divergent activation of the UPR has been previously observed in different contexts<sup>62,63</sup>. Activation of IRE1 and PERK sensors could indicate an endeavour of the cell to survive the ER stress caused by the transient accumulation of precursor forms of LOXL2. Phosphorylation of eIF2 $\alpha$  could diminish protein translation while spliced XBP1 would increase the ER-associated maturation machinery and raise the secretion potential of the ER<sup>44,64</sup>. Nevertheless, the fact that the specific inhibition of IRE1 completely abolished LOXL2-dependent induction of several EMT-TFs indicates that IRE1-XBP1 is the main UPR branch involved in the EMT process mediated by LOXL2, and this is further supported by the binding of spliced XBP1 to EMT-TFs promoters. LOXL2 mediated induction of EMT-TFs could also be confirmed at promoter level for at least *SNAI2* and *TCF3* genes. Interestingly, both promoters are not or only slightly activated by tunicamycin, suggesting that tunicamycin is a weaker activator of the IRE1-XBP1

branch than LOXL2/ $\Delta$ LOXL2 in the analysed conditions. On the other hand, the functional consequences of LOXL2-mediated PERK activation for tumour progression remain to be investigated as well as potential additional mechanisms of LOXL2-mediated IRE1-XBP1 activation as recently reported for oestrogen induced XBP1 in some breast cancer types<sup>65</sup>.

It is remarkable that  $\Delta$ LOXL2, an inactive mutant lacking 120 amino acids of the catalytic domain<sup>14</sup> is able to upregulate Xbp1 gene targets at even higher levels than LOXL2 (Fig. 4a). Although we do not have experimental data to explain this fact, a plausible explanation could be that the interaction of  $\Delta$ LOXL2 with HSPA5 is stronger than that of the wild type, therefore inducing a stronger ER stress. This observation also opens the possibility that overexpression of different mutant proteins could provoke the same or similar phenotype than  $\Delta$ LOXL2.

Numerous previous works have shown the importance of UPR in different diseases and in cancer<sup>44</sup>. Concerning breast cancer, a recent report has shown that XBP1 is activated in triple-negative breast cancer. In this case, XBP1 controls the HIF1 $\alpha$  transcriptional program to promote tumorigenicity, progression and recurrence of triple-negative tumours<sup>66</sup>. Additionally, in breast cancer cell lines, overexpression of XBP1 promotes EMT<sup>67</sup>. Noticeably, in the present report, we show that LOXL2 overexpression upregulates the expression of several EMT-TFs due to IRE1-XBP1 activation which in turn promote EMT; in fact, several EMT-TFs are direct XBP1 target genes. Moreover, inhibition of IRE1 blocks LOXL2 ability to induce a full EMT program, thus functionally linking LOXL2-IRE1-UPR and EMT. Together, these observations would also suggest that a positive feed-back loop between HIF1 $\alpha$ , LOXL2-XBP1 and EMT can operate at least in some tumour contexts that deserve further studies.

In conclusion, we propose that, at least in laryngeal squamous cell carcinomas and basal-like breast carcinomas, the observed intracellular LOXL2 staining pattern corresponds to protein temporally retained in the ER that activates the IRE1-XBP1 and PERK branches of the UPR. LOXL2-activated XBP1 directly promotes upregulation of EMT-TFs that in turn would favour the high aggressiveness and metastasis of those tumour types.

## Methods

**Cell culture.** Human HEK293T, MDA-MB-231 and Hs578T, mouse Eo771 and dog MDCK-II cell lines were obtained from the American Type Culture Collection and grown in DMEM media (Gibco), supplemented with 10% foetal bovine serum, 10 mmol/L glutamine (Life Technologies) and 1% penicillin/streptomycin (Invitrogen). All cell lines were grown at 37 °C in a humidified 5% CO<sub>2</sub> atmosphere. MDCK-II cells stably expressing LOXL2-HA and the  $\Delta$ LOXL2-Flag catalytically inactive mutant have been previously described<sup>14</sup>. Eo771 and MDA-MB-231 cells silenced for LOXL2 expression (shLOXL2) have also been described<sup>16,59</sup>.

For chemical ER stress induction, cells were treated with 1  $\mu$ g/ml tunicamycin for 16 h (promoter assays) or 24 h (western blot, qPCR and RT-PCR). For IRE1 inhibition and analysis in RT-PCR assays, cells were treated with 20  $\mu$ M 4 $\mu$ 8 C for 24 h. For tetracycline-inducible LOXL2 expression, MDCK-II cells were grown in culture medium supplemented with doxycycline (100 ng/ml) and treated with 20  $\mu$ M 4 $\mu$ 8 C for the indicated time.

**Generation of cells conditionally expressing LOXL2.** MDCK-II cells were transfected with the plasmid pTet-On (Clontech) coding for the reverse tet-responsive transcriptional activator (rtTA)<sup>68</sup> and stable clones were selected. Selected stable Tet-On cell line was further transfected with plasmid pTRE2hyg-LOXL2 generating an inducible LOXL2 expressing cell line responsive to doxycycline. pTRE2hyg-LOXL2 is a derivative of the pTRE2hyg plasmid (Clontech) and expresses LOXL2 under the control of the Tet-responsive P<sub>hCMV-1</sub> promoter. This plasmid was generated by cloning a 2.3 Kb *NheI-SalI* fragment containing a Flag-tagged version of the human LOXL2 cDNA into the corresponding *NheI* and *SalI* sites of the pTRE2hyg multiple cloning site. The 2.3 Kb *NheI-SalI* fragment was generated from plasmid pcDNA3-hLOXL2-Flag<sup>13</sup> that was digested with *HindIII*, the *HindIII* site is unique in the plasmid and is located 5' with respect to the LOXL2 cDNA. After digestion, the ends were made blunt with Klenow and ligated. This manipulation destroys the original *HindIII* sites and creates a *NheI* site.

**Chromatin Immunoprecipitation (ChIP) assay.** ChIP assays were performed in HEK293T cells transiently transfected with a Flag-tagged version of the processed XBP1 (*XBP1p*) (Addgene), using formaldehyde before sonication, as described<sup>14</sup>. For detection of interaction of tagged Xbp1 with endogenous promoters, anti-Flag M2 affinity gel (Sigma), or unspecific mouse IgG (Jackson ImmunoResearch Laboratories) and Protein G-agarose beads (Sigma) were used. Promoter fragments of the different EMT-TFs were amplified using the primers described in Supplementary Table 1.

**Promoter assays.** Luciferase reporter assays were performed as described<sup>69</sup>. Briefly, transfections were carried out in the presence of 50 ng of empty pcDNA3 vector, LOXL2,  $\Delta$ LOXL2, ANXA2 or XBP1p (Addgene) expression vectors, 200 ng of the indicated promoters and 10 ng of pCMV- $\beta$ -gal as control of transfection efficiency. Luciferase and  $\beta$ -galactosidase activities were measured using the luciferase and  $\beta$ -Glo assay substrates (Promega) and normalized to the promoter activity detected in cells transfected with pcDNA3 empty vector. The p5xUPRE-GL3 (*UPRE*) and pGL3-GRP78P(-132)-luc (*ERSE*) reporter plasmids were gifts from Dr. K. Mori (Kyoto University, Kitashirakawa-Oiwake, Sakyo-ku, Kyoto, Japan). Plasmid expressing human ANXA2 was a gift of Dr. E. Colas (Vall d'Hebron Institute of Research, Barcelona, Spain). *SNAIL2* and *TCF3* promoters were gifts from Dr. P. Savagner (Centre de Recherche en Cancerologie, CRLC, Montpellier, France) and Dr. J. Mizuguchi (School of Medicine, University of Tokyo, Japan), respectively. When indicated, tunicamycin was added as described above. All experiments were performed at least four times on triplicate samples.

**RT-PCR.** Total RNA was extracted with Trizol reagent (Invitrogen) followed by phenol-chloroform extraction protocol. cDNA synthesis (Superscript II RNase H reverse transcriptase, Invitrogen) was prepared from 2  $\mu$ g of RNA and amplified with REExtract-N-Amp PCR Reaction Mix (Sigma) using the specific primers described in Supplementary Table 2. Amplified fragments were separated on TAE-agarose gel and stained with SYBR safe (Invitrogen).



**qPCR.** Quantitative real-time PCR was performed with Iq5 BIORAD Multicolour Real-Time PCR Detection System and the associated software (iQ5 Optical System Software), using the manufacturer's recommended conditions. Each reaction was performed in biological triplicates with 20 ng of cDNA by using Syber Green reagent (Quanta Biosciences). Values were relativized to GAPDH levels (primer pairs are listed in Supplementary Table 3).

**Microarray.** Microarray experiments were performed using Human Whole Genome V2 4\*44 K array G4845A (Agilent technologies). Three independent passages from MDCK-II-LOXL2 and MDCK-II- $\Delta$ LOXL2 cells were used, and MDCK-II transfected with empty pcDNA3 vector were used as control. Total RNA was extracted and purified as described<sup>16</sup>. Microarray labelling and hybridization was performed using the Low RNA Linear Amplification Kit and the *In Situ* Hybridization Kit Plus (Agilent technologies), respectively, following manufacturer's protocol. After hybridization and washing, the slides were scanned in an Axon GenePix Scanner (Axon Instruments) and analysed using Feature Extraction Software 10.0 (Agilent technologies). RNA samples from independent MDCK-II-LOXL2 and - $\Delta$ LOXL2-stably transfected cells were labelled with Cy5-dUTP and equal concentrations of RNA from control cells were labelled with Cy3-dUTP. Differentially expressed genes were selected using the False Discovery Rate (FDR) method with an adjusted p-value < 0.2. Microarray raw data tables have been deposited in the Gene Expression Omnibus under the accession number GSE90605 (submitter G. M.-B.).

**Confocal Immunofluorescence.** Immunofluorescence analysis was performed as described<sup>14,69</sup> on cells grown on coverslips, fixed in paraformaldehyde and permeabilized with 0.05% Triton-X100. Cells were incubated for 2 h at 37 °C in a humidified chamber with the primary and secondary antibodies, described in Supplementary Table 4. Phalloidin-647 (Amersham) was used for F-actin stain. Confocal microscopy analyses were performed using a Zeiss Spectral LSM710 microscope (x40 oil objective) and Zen2009 software.

**Western blots.** Western blot analyses were performed as previously described<sup>69</sup>. The primary and secondary antibodies used are described in Supplementary Table 4. The cropped images for western blots are shown in the main figures; however, the uncropped scan for each blot is shown in the Supplementary Fig. 8.

**Subcellular fractionation.** Cells were scraped from culture plates into ice-cold PBS, washed with the same buffer and collected by centrifugation. Cell pellets were then suspended in HB buffer (10 mM Hepes-NaOH, pH7.4, 1 mM EDTA, 1 mM DTT) plus 0.25 M sucrose and protease inhibitor cocktail (Complete, EDTA-free, Roche Diagnostics), lysed with 30 strokes of a Dounce homogenizer and centrifuged at 600 × g for 10 min. The post-nuclear supernatant was centrifuged at 160,000 × g for 60 min to obtain a total membrane fraction that was homogenized in 2 ml 35% iodixanol (OptiPrep™, Sigma) in HB buffer and overlaid by 2.25 ml 30%, 2.25 ml 20%, 2.25 ml 10% and 1.3 ml 2.5% iodixanol. After centrifugation at 4 °C for 16 h at 28,000 × g in a SW41Ti rotor (Beckman), 0.7 ml fractions were collected from top to bottom of the gradient, 10% TCA precipitated and solubilized in Laemmli loading buffer.

**Immunoprecipitation.** HEK293T-cells were transiently transfected with control pcDNA3 or pcDNA3-hLOXL2-Flag. Cell extracts were obtained using IPH buffer (50 mM Tris-HCl pH 8.0, 150 mM NaCl, 5 mM EDTA, 0.5% NP-40) supplemented with proteases and phosphatases inhibitors (2 mM PMSE, 2 µg/ml leupeptin, 20 ng/ml aprotinin, 1 mM sodium orthovanadate). One mg of protein lysate was pre-cleared with protein G-agarose beads (Sigma) for 3 h and then subjected to immunoprecipitation with anti-Flag M2 affinity gel (Sigma) for 5 h at 4 °C. Precipitates were washed five times with IPH buffer (1 ml) and then suspended in 100 µl of the same buffer for proteomic analysis.

**Co-Immunoprecipitation.** Total membranes (250 µg of protein) from Hs578T cells were solubilized in TXNE buffer (10 mM Tris-HCl pH 7.5, 150 mM NaCl, 2 mM EDTA, 1% Triton X-100) plus protease inhibitor cocktail (Roche) for 1 h at 4 °C. The solubilized membranes were immunoprecipitated by incubation for 3 h at 4 °C with anti-HSPA5 bound to Dynabeads Protein G (ThermoFisher) in TXNE buffer. The immune complexes bound were eluted, after extensive washing with the same buffer, by incubation 5 min at 95 °C in Laemmli sample buffer. Proteins in the eluted fraction were separated by SDS-polyacrylamide gel electrophoresis and analysed by immunoblot. Co-immunoprecipitations of HEK293T cells expressing ectopically LOXL2 or  $\Delta$ LOXL2 were performed as described<sup>14</sup>.

**Statistical analysis.** P-values were generated using Student's t-test (unpaired, 2-tailed); a p value < 0.05 was considered statistically significant. Data are presented as standard error of the mean (s.e.m.).

## References

1. Thiery, J. P., Acloque, H., Huang, R. Y. & Nieto, M. A. Epithelial-mesenchymal transitions in development and disease. *Cell* **139**, 871–890, doi: 10.1016/j.cell.2009.11.007 (2009).
2. De Craene, B. & Berx, G. Regulatory networks defining EMT during cancer initiation and progression. *Nat Rev Cancer* **13**, 97–110, doi: 10.1038/nrc3447 (2013).
3. Kalluri, R. & Weinberg, R. A. The basics of epithelial-mesenchymal transition. *J Clin Invest* **119**, 1420–1428, doi: 10.1172/JCI39104 (2009).
4. Mani, S. A. *et al.* The epithelial-mesenchymal transition generates cells with properties of stem cells. *Cell* **133**, 704–715, doi: 10.1016/j.cell.2008.03.027 (2008).
5. Moreno-Bueno, G., Portillo, F. & Cano, A. Transcriptional regulation of cell polarity in EMT and cancer. *Oncogene* **27**, 6958–6969, doi: 10.1038/onc.2008.346 (2008).
6. Nieto, M. A. Epithelial plasticity: a common theme in embryonic and cancer cells. *Science* **342**, 1234850, doi: 10.1126/science.1234850 (2013).
7. Nieto, M. A. & Cano, A. The epithelial-mesenchymal transition under control: global programs to regulate epithelial plasticity. *Semin Cancer Biol* **22**, 361–368, doi: 10.1016/j.semcancer.2012.05.003 (2012).

8. Nieto, M. A. The ins and outs of the epithelial to mesenchymal transition in health and disease. *Annu Rev Cell Dev Biol* **27**, 347–376, doi: 10.1146/annurev-cellbio-092910-154036 (2011).
9. Peinado, H., Olmeda, D. & Cano, A. Snail, Zeb and bHLH factors in tumour progression: an alliance against the epithelial phenotype? *Nat Rev Cancer* **7**, 415–428, doi: 10.1038/nrc2131 (2007).
10. Lamouille, S., Xu, J. & Derynck, R. Molecular mechanisms of epithelial-mesenchymal transition. *Nat Rev Mol Cell Biol* **15**, 178–196, doi: 10.1038/nrm3758 (2014).
11. Fischer, K. R. *et al.* Epithelial-to-mesenchymal transition is not required for lung metastasis but contributes to chemoresistance. *Nature* **527**, 472–476, doi: 10.1038/nature15748 (2015).
12. Zheng, X. *et al.* Epithelial-to-mesenchymal transition is dispensable for metastasis but induces chemoresistance in pancreatic cancer. *Nature* **527**, 525–530, doi: 10.1038/nature16064 (2015).
13. Peinado, H. *et al.* A molecular role for lysyl oxidase-like 2 enzyme in snail regulation and tumor progression. *EMBO J* **24**, 3446–3458, doi: 10.1038/sj.emboj.7600781 (2005).
14. Cuevas, E. P. *et al.* LOXL2 catalytically inactive mutants mediate epithelial-to-mesenchymal transition. *Biol Open* **3**, 129–137, doi: 10.1242/bio.20146841 (2014).
15. Peinado, H. *et al.* Lysyl oxidase-like 2 as a new poor prognosis marker of squamous cell carcinomas. *Cancer Res* **68**, 4541–4550, doi: 10.1158/0008-5472.CAN-07-6345 (2008).
16. Moreno-Bueno, G. *et al.* Lysyl oxidase-like 2 (LOXL2), a new regulator of cell polarity required for metastatic dissemination of basal-like breast carcinomas. *EMBO Mol Med* **3**, 528–544, doi: 10.1002/emmm.201100156 (2011).
17. Cano, A., Santamaria, P. G. & Moreno-Bueno, G. LOXL2 in epithelial cell plasticity and tumor progression. *Future Oncol* **8**, 1095–1108, doi: 10.2217/fo.12.105 (2012).
18. Barker, H. E., Cox, T. R. & Erler, J. T. The rationale for targeting the LOX family in cancer. *Nat Rev Cancer* **12**, 540–552, doi: 10.1038/nrc3319 (2012).
19. Finney, J., Moon, H. J., Ronnebaum, T., Lantz, M. & Mure, M. Human copper-dependent amine oxidases. *Arch Biochem Biophys* **546**, 19–32, doi: 10.1016/j.abb.2013.12.022 (2014).
20. Grau-Bove, X., Ruiz-Trillo, I. & Rodriguez-Pascual, F. Origin and evolution of lysyl oxidases. *Sci Rep* **5**, 10568, doi: 10.1038/srep10568 (2015).
21. Lucero, H. A. & Kagan, H. M. Lysyl oxidase: an oxidative enzyme and effector of cell function. *Cell Mol Life Sci* **63**, 2304–2316, doi: 10.1007/s00018-006-6149-9 (2006).
22. Trackman, P. C. Enzymatic and non-enzymatic functions of the lysyl oxidase family in bone. *Matrix Biol*, doi: 10.1016/j.matbio.2016.01.001 (2016).
23. Martinez, V. G., Moestrup, S. K., Holmskov, U., Mollenhauer, J. & Lozano, F. The conserved scavenger receptor cysteine-rich superfamily in therapy and diagnosis. *Pharmacol Rev* **63**, 967–1000, doi: 10.1124/pr.111.004523 (2011).
24. Hohenester, E., Sasaki, T. & Timpl, R. Crystal structure of a scavenger receptor cysteine-rich domain sheds light on an ancient superfamily. *Nat Struct Biol* **6**, 228–232, doi: 10.1038/6669 (1999).
25. Xu, L. *et al.* Post-translational modifications of recombinant human lysyl oxidase-like 2 (rhLOXL2) secreted from *Drosophila* S2 cells. *J Biol Chem* **288**, 5357–5363, doi: 10.1074/jbc.C112.421768 (2013).
26. Barker, H. E. *et al.* LOXL2-mediated matrix remodeling in metastasis and mammary gland involution. *Cancer Res* **71**, 1561–1572, doi: 10.1158/0008-5472.CAN-10-2868 (2011).
27. de Jong, O. G., van Balkom, B. W., Gremmels, H. & Verhaar, M. C. Exosomes from hypoxic endothelial cells have increased collagen crosslinking activity through up-regulation of lysyl oxidase-like 2. *J Cell Mol Med* **20**, 342–350, doi: 10.1111/jcmm.12730 (2016).
28. Bignon, M. *et al.* Lysyl oxidase-like protein-2 regulates sprouting angiogenesis and type IV collagen assembly in the endothelial basement membrane. *Blood* **118**, 3979–3989, doi: 10.1182/blood-2010-10-313296 (2011).
29. Yoon, J. H. *et al.* Proteomic analysis of hypoxia-induced U373MG glioma secretome reveals novel hypoxia-dependent migration factors. *Proteomics* **14**, 1494–1502, doi: 10.1002/pmic.201300554 (2014).
30. Naba, A., Clauser, K. R., Lamar, J. M., Carr, S. A. & Hynes, R. O. Extracellular matrix signatures of human mammary carcinoma identify novel metastasis promoters. *Elife* **3**, e01308, doi: 10.7554/eLife.01308 (2014).
31. Millanes-Romero, A. *et al.* Regulation of heterochromatin transcription by Snail1/LOXL2 during epithelial-to-mesenchymal transition. *Mol Cell* **52**, 746–757, doi: 10.1016/j.molcel.2013.10.015 (2013).
32. Moon, H. J. *et al.* MCF-7 cells expressing nuclear associated lysyl oxidase-like 2 (LOXL2) exhibit an epithelial-to-mesenchymal transition (EMT) phenotype and are highly invasive *in vitro*. *J Biol Chem* **288**, 30000–30008, doi: 10.1074/jbc.C113.502310 (2013).
33. Baker, A. M. *et al.* The role of lysyl oxidase in SRC-dependent proliferation and metastasis of colorectal cancer. *J Natl Cancer Inst* **103**, 407–424, doi: 10.1093/jnci/djq569 (2011).
34. Maki, J. M. Lysyl oxidases in mammalian development and certain pathological conditions. *Histol Histopathol* **24**, 651–660 (2009).
35. Nishioka, T., Eustace, A. & West, C. Lysyl oxidase: from basic science to future cancer treatment. *Cell Struct Funct* **37**, 75–80 (2012).
36. Payne, S. L., Hendrix, M. J. & Kirschmann, D. A. Paradoxical roles for lysyl oxidases in cancer—a prospect. *J Cell Biochem* **101**, 1338–1354, doi: 10.1002/jcb.21371 (2007).
37. Trackman, P. C. Lysyl Oxidase Isoforms and Potential Therapeutic Opportunities for Fibrosis and Cancer. *Expert Opin Ther Targets*, 1–11, doi: 10.1517/14728222.2016.1151003 (2016).
38. Xiao, Q. & Ge, G. Lysyl oxidase, extracellular matrix remodeling and cancer metastasis. *Cancer Microenviron* **5**, 261–273, doi: 10.1007/s12307-012-0105-z (2012).
39. Ellgaard, L. & Helenius, A. Quality control in the endoplasmic reticulum. *Nat Rev Mol Cell Biol* **4**, 181–191, doi: 10.1038/nrm1052 (2003).
40. Wickner, W. & Schekman, R. Protein translocation across biological membranes. *Science* **310**, 1452–1456, doi: 10.1126/science.1113752 (2005).
41. Ron, D. & Walter, P. Signal integration in the endoplasmic reticulum unfolded protein response. *Nat Rev Mol Cell Biol* **8**, 519–529, doi: 10.1038/nrm2199 (2007).
42. Ma, Y. & Hendershot, L. M. The role of the unfolded protein response in tumour development: friend or foe? *Nat Rev Cancer* **4**, 966–977, doi: 10.1038/nrc1505 (2004).
43. Ozcan, L. & Tabas, I. Role of endoplasmic reticulum stress in metabolic disease and other disorders. *Annu Rev Med* **63**, 317–328, doi: 10.1146/annurev-med-043010-144749 (2012).
44. Wang, M. & Kaufman, R. J. The impact of the endoplasmic reticulum protein-folding environment on cancer development. *Nat Rev Cancer* **14**, 581–597, doi: 10.1038/nrc3800 (2014).
45. Bernales, S., Papa, F. R. & Walter, P. Intracellular signaling by the unfolded protein response. *Annu Rev Cell Dev Biol* **22**, 487–508, doi: 10.1146/annurev.cellbio.21.122303.120200 (2006).
46. Schroder, M. & Kaufman, R. J. The mammalian unfolded protein response. *Annu Rev Biochem* **74**, 739–789, doi: 10.1146/annurev.biochem.73.011303.074134 (2005).
47. Bertolotti, A., Zhang, Y., Hendershot, L. M., Harding, H. P. & Ron, D. Dynamic interaction of BiP and ER stress transducers in the unfolded-protein response. *Nat Cell Biol* **2**, 326–332, doi: 10.1038/35014014 (2000).
48. Yoshida, H., Matsui, T., Yamamoto, A., Okada, T. & Mori, K. XBP1 mRNA is induced by ATF6 and spliced by IRE1 in response to ER stress to produce a highly active transcription factor. *Cell* **107**, 881–891 (2001).

49. Harding, H. P., Zhang, Y., Bertolotti, A., Zeng, H. & Ron, D. Perk is essential for translational regulation and cell survival during the unfolded protein response. *Mol Cell* **5**, 897–904 (2000).
50. Wang, Y. *et al.* Activation of ATF6 and an ATF6 DNA binding site by the endoplasmic reticulum stress response. *J Biol Chem* **275**, 27013–27020, doi: 10.1074/jbc.M003322200 (2000).
51. Ye, J. *et al.* ER stress induces cleavage of membrane-bound ATF6 by the same proteases that process SREBPs. *Mol Cell* **6**, 1355–1364 (2000).
52. Yamamoto, K., Yoshida, H., Kokame, K., Kaufman, R. J. & Mori, K. Differential contributions of ATF6 and XBP1 to the activation of endoplasmic reticulum stress-responsive cis-acting elements ERSE, UPRE and ERSE-II. *J Biochem* **136**, 343–350, doi: 10.1093/jb/mvh122 (2004).
53. Kaufman, R. J. Stress signaling from the lumen of the endoplasmic reticulum: coordination of gene transcriptional and translational controls. *Genes Dev* **13**, 1211–1233 (1999).
54. Acosta-Alvear, D. *et al.* XBP1 controls diverse cell type- and condition-specific transcriptional regulatory networks. *Mol Cell* **27**, 53–66, doi: 10.1016/j.molcel.2007.06.011 (2007).
55. Lu, P. D., Harding, H. P. & Ron, D. Translation reinitiation at alternative open reading frames regulates gene expression in an integrated stress response. *J Cell Biol* **167**, 27–33, doi: 10.1083/jcb.200408003 (2004).
56. Vattam, K. M. & Wek, R. C. Reinitiation involving upstream ORFs regulates ATF4 mRNA translation in mammalian cells. *Proc Natl Acad Sci USA* **101**, 11269–11274, doi: 10.1073/pnas.0400541101 (2004).
57. Shoulder, M. D. *et al.* Stress-independent activation of XBP1s and/or ATF6 reveals three functionally diverse ER proteostasis environments. *Cell Reports* **3**, 1279–1292 doi: 10.1016/j.celrep.2013.03.024 (2013).
58. Tomasio, S. M., Harding, H. P., Ron, D., Cross, B. C. & Bond, P. J. Selective inhibition of the unfolded protein response: targeting catalytic sites for Schiff base modification. *Mol Biosyst* **9**, 2408–2416, doi: 10.1039/c3mb70234k (2013).
59. Canesin, G. *et al.* Lysyl oxidase-like 2 (LOXL2) and E47 EMT factor: novel partners in E-cadherin repression and early metastasis colonization. *Oncogene* **34**, 951–964, doi: 10.1038/ncr.2014.23 (2015).
60. Gupta, G. P. & Massague, J. Cancer metastasis: building a framework. *Cell* **127**, 679–695, doi: 10.1016/j.cell.2006.11.001 (2006).
61. Schietke, R. *et al.* The lysyl oxidases LOX and LOXL2 are necessary and sufficient to repress E-cadherin in hypoxia: insights into cellular transformation processes mediated by HIF-1. *J Biol Chem* **285**, 6658–6669, doi: 10.1074/jbc.M109.042424 (2010).
62. Sheng, X. *et al.* Divergent androgen regulation of unfolded protein response pathways drives prostate cancer. *EMBO Mol Med* **7**, 788–801, doi: 10.15252/emmm.201404509 (2015).
63. Wang, G. *et al.* ERLIN2 promotes breast cancer cell survival by modulating endoplasmic reticulum stress pathways. *BMC Cancer* **12**, 225, doi: 10.1186/1471-2407-12-225 (2012).
64. Wang, M. & Kaufman, R. J. Protein misfolding in the endoplasmic reticulum as a conduit to human disease. *Nature* **529**, 326–335, doi: 10.1038/nature17041 (2016).
65. Gupta, A. *et al.* NCOA3 coactivator is a transcriptional target of XBP1 and regulates PERK-eIF2 $\alpha$ -ATF4s signalling in breast cancer. *Oncogene* **35**, 5860–5871, doi: 10.1038/ncr.2016.121 (2016).
66. Chen, X. *et al.* XBP1 promotes triple-negative breast cancer by controlling the HIF1 $\alpha$  pathway. *Nature* **508**, 103–107, doi: 10.1038/nature13119 (2014).
67. Li, H. *et al.* XBP1 induces snail expression to promote epithelial- to-mesenchymal transition and invasion of breast cancer cells. *Cell Signal* **27**, 82–89, doi: 10.1016/j.cellsig.2014.09.018 (2015).
68. Baron, U., Gossen, M. & Bujard, H. Tetracycline-controlled transcription in eukaryotes: novel transactivators with graded transactivation potential. *Nucleic Acids Res* **25**, 2723–2729 (1997).
69. Moreno-Bueno, G. *et al.* The morphological and molecular features of the epithelial-to-mesenchymal transition. *Nat Protoc* **4**, 1591–1613, doi: 10.1038/nprot.2009.152 (2009).
70. Shang, J. & Lehrman, M. A. Discordance of UPR signalling by ATF6 and Ire1p-XBP1 with levels of target transcript. *Biochem Biophys Res Comm* **317**, 390–296, doi: 10.1016/j.bbrc.2004.03.058 (2004).

## Acknowledgements

We would like to thank members of Amparo Cano's lab for helpful discussions. We also thank our colleagues who provided reagents. This work has been supported by grants from the Spanish Ministerio de Economía y Competitividad SAF2013-44739-R and SAF2016-76504-R (AC and FP), the Spanish Instituto de Salud Carlos III [(RETIC-RD12/0036/0007 (AC), PI13/00132 (GMB), CB16/12/00295 (AC), CIBERONC (AC)] (all of them partly supported from EU-FEDER funds), and Worldwide Cancer Research (WWCR, formerly AICR) AICR 12-1057 (AC). EPC and VS were founded by postdoctoral and technician contracts, respectively, from SAF2013-44739-R and WWCR grants.

## Author Contributions

F.P. and A.C. designed the experiments. E.P.C., P.E., and MJM, performed the experiments with the help of V.S. E.P.C., P.E., M.J.M., F.P. and A.C. analysed the data. G.M.B. performed the microarrays analysis. F.P. and A.C. wrote the manuscript. E.P.C., P.E., M.J.M. and G.M.B. revised the manuscript.

## Additional Information

**Supplementary information** accompanies this paper at <http://www.nature.com/srep>

**Competing Interests:** The authors declare no competing financial interests.

**How to cite this article:** Cuevas, E. P. *et al.* LOXL2 drives epithelial-mesenchymal transition via activation of IRE1-XBP1 signalling pathway. *Sci. Rep.* **7**, 44988; doi: 10.1038/srep44988 (2017).

**Publisher's note:** Springer Nature remains neutral with regard to jurisdictional claims in published maps and institutional affiliations.



This work is licensed under a Creative Commons Attribution 4.0 International License. The images or other third party material in this article are included in the article's Creative Commons license, unless indicated otherwise in the credit line; if the material is not included under the Creative Commons license, users will need to obtain permission from the license holder to reproduce the material. To view a copy of this license, visit <http://creativecommons.org/licenses/by/4.0/>

© The Author(s) 2017